Phase-regularized polygon computer-generated holograms

Dajeong Im,¹ Eunkyoung Moon,¹ Yohan Park,¹ Deokhwan Lee,² Joonku Hahn,³ and Hwi Kim¹,*

¹ICT Convergence Technology for Health & Safety and Department of Electronics and Information Engineering, Korea University, 2511 Sejong-ro, Sejong 339-700, South Korea

²Lily S&C Co., Ltd., Teheran-ro 37 gil, Gangnam-gu Seoul 135-915, South Korea

³School of Electronics Engineering, Kyungpook National University, 1370 Buk-Gu, Sankyuk-Dong, Daegu 702-701, South Korea

*Corresponding author: hwikim@korea.ac.kr

The dark-line defect problem in the conventional polygon computer-generated hologram (CGH) is addressed. To resolve this problem, we clarify the physical origin of the defect and address the concept of phase-regularization. A novel synthesis algorithm for a phase-regularized polygon CGH for generating photorealistic defect-free holographic images is proposed. The optical reconstruction results of the phase-regularized polygon CGHs without the dark-line defects are presented.   © 2014 Optical Society of America

OCIS codes: (090.1995) Digital holography; (090.2870) Holographic display.

http://dx.doi.org/10.1364/OL.39.003642

Holographic three-dimensional (3D) displays have been actively researched and are currently considered as the ultimate 3D display [1–3]. At present, the design of a practical holographic 3D display is still challenging from both hardware and software perspectives [4]. Considerable research effort is being devoted to not only the advancement of spatial light modulator (SLM) technology with the sub-micron pixel size and ultrahigh resolution, but also the improvement of algorithms for creating computer-generated holograms (CGHs) to achieve real-time computational performance [5,6] and photorealistic image quality [1,7–13].

In the context of algorithm development, the CGH representation theory is an important research area with the objective being to represent the photorealistic holographic 3D scenes. The representation of these realistic CGH images relies on techniques such as texturing, shading, and rendering. There have been several theoretical studies conducted on the theory of CGH representation [9–13]. The point cloud model has been widely used to compute the CGHs of 3D objects [4]. To correctly represent realistic objects using this method, a highly dense point cloud is necessary, so computational efficiency is crucial.

The point cloud CGH method is considered inappropriate when representing sleek or metallic surfaces because of the diffusive nature of the point cloud modeled surface. This diffusive surface can be viewed as a sort of speckle pattern, which appears as a collection of many arbitrarily curved and crossed dark-line defects. The polygon CGH method is a relatively new method and advantageous for the realistic and computational efficient representation of 3D scenes [7–9]. Using this representation method, which is also commonly used in the field of computer graphics, the 3D objects are represented by plural triangular facets. The holographic 3D image light field is mathematically expressed by the angular spectrum integral. The triangular facet is a computational unit and is reconstructed in the form of a non-diffusive continuous facet.

The conventional polygon CGH method exhibits a dark-line defect, apparent as a kind of speckle pattern, which occurs at the borders of the adjacent triangular facets. Figure 1 shows the numerical observation of a holographic 3D image generated by the conventional polygon CGH synthesis method. The borders of adjacent triangular facets appear as dark lines and are referred to as dark-line defects. The dark-line defects are clearly observed on the surface of the 3D objects, not only in numerical observation, such as in Fig. 1(a), but also in experimental observation in Fig. 1(b). This defect, to our knowledge, is an unresolved issue of the polygon CGH algorithm.

In this Letter, we unravel the physical origin of the dark-line defect and propose a novel polygon CGH synthesis algorithm for generating photorealistic defect-free holographic images. The physical origin of the dark-line defect is inferred to be a wide-angle diffraction caused by an abrupt wavefront change at the borders of the
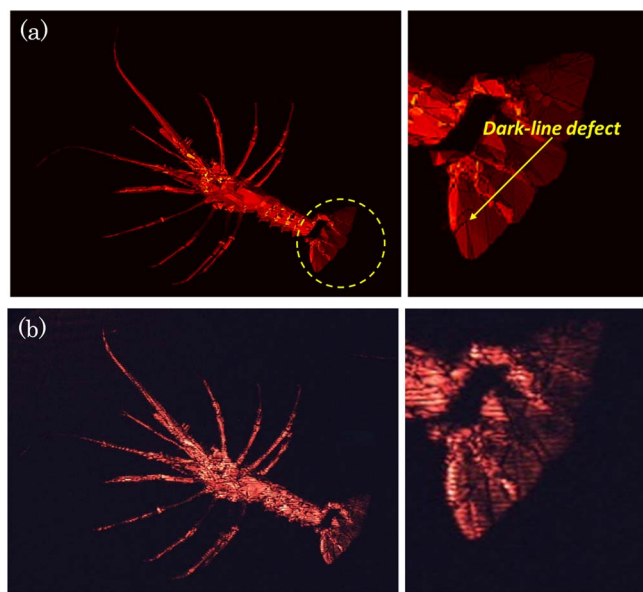

Fig. 1.   Dark-line defects observed in (a) numerical and (b) experimental reconstructions of a holographic 3D image calculated by the conventional polygon CGH method.

adjacent triangle facets with the unparallel surface normals represented in Fig. 2. The abrupt change at the polygon boundaries causes the carrier wave passing through the triangular aperture to be diffracted. The piecewise continuity, as well as discontinuity, i.e., phase mismatch, in wavefront can also induce wide-angle diffraction as represented in Fig. 2(a). The observer recognizes the diffraction by the abrupt change in the wavefront profile. To prevent this change, the wavefront needs to maintain smoothness at the polygon boundaries. This concept, explored in this Letter, will be referred to as phase-regularization. Figure 2(a) compares the wavefront profiles of the holographic fields generated by the conventional method and the proposed phase-regularization method. In Fig. 2(b), the phase matching condition for the carrier wave convergent toward the viewing window of the observer is illustrated. ϕ_1 and ϕ_2 are the phase values at two separate positions on the surface of a 3D object. The imaged voxels corresponding to those points are formed in the retina space. Let the phase values of the two imaged voxels be ψ_1 and ψ_2. The optical path length between two voxel pairs, $\phi_1 - \psi_1$ and $\phi_2 - \psi_2$, may be different. Intuitively, we can see that the wavefront should be aligned in the retina space to prevent the dark-line defects from appearing, meaning that, in this phase matching condition [8], ψ_1 should be equal to ψ_2. In this case, the phase values on the object surface, ϕ_1 and ϕ_2, do not have to be equal.

In this Letter, we propose a novel synthesis algorithm for a phase-regularized polygon CGH to resolve the dark-line defect problem and synthesize the photorealistic defect-free holographic images. The proposed algorithm is based on phase-regularization. The CGH is calculated for the projected object floating in the retina space, rather than the free space. The functional effects of this setup are summarized as, first, wavefront lineup in the retina plane and, second, rendering a piecewise continuous wavefront at the borders of the triangular facets.

In Fig. 3(a), the optical system schematic of the eye observation of a holographic 3D image is shown. An observer watches the holographic image volume created by the holographic display with, but here the eye is simply modeled by an optical imaging system. The CGH is supposed to float a 3D object around at $z = z_{center}$. The CGH plane (x_1, y_1), the eye lens plane (u, v), and the retina plane (x_2, y_2) are defined as shown in Fig. 3(a). The field lens with a focal length of F is placed behind of the CGH plane as shown in Fig. 3(b), and then the viewing window is set at the position distant from the CGH plane by F. If it is assumed that the observer's focus is on the center of object $z = z_{center}$, the focal length of the eye lens is tuned to the center of the object, and then given by:

$$f_{eye} = 1/[1/(F - z_{center}) + 1/d_{eye}], \quad (1a)$$

where d_{eye} is the distance between the eye lens and the retina plane. Let us consider a corner point of a triangle facet $(x_{object}, y_{object}, z_{object})$. This point is transferred to the retina space by:

$$(x_{retina}, y_{retina}, z_{retina})$$
$$= (-x_{object}D_2/D_1, -y_{object}D_2/D_1, D_2 - d_{eye}), \quad (1b)$$

where $D_1 = F - z_{object}$ and $D_2 = 1/[1/f_{eye} - 1/D_1]$.

An important feature in the eye imaging process is that the axial magnification ratio is substantially smaller than the transversal magnification ratio as indicated in Fig. 2(a). As a result, the 3D object in the retina space looks thinner than the 3D object in the object space. This geometrical transformation results because the included angles of adjacent triangular facets in the retina space become larger than those of adjacent triangular facets in the object space, as emphasized in Fig. 2(a).
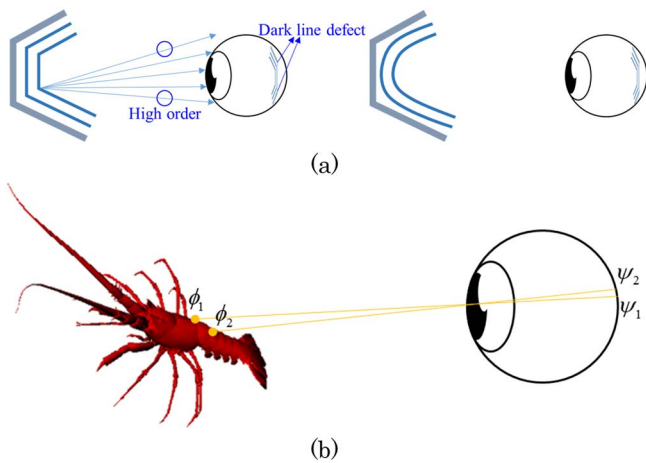

Fig. 2. Concept of phase-regularization. (a) Piecewise continuity with an abrupt change in the wavefront accompanies wide-angle edge diffraction, inducing the dark-line defect. In contrast, an optical wave with a smoothly rendered wavefront can depress the edge diffraction and therefore does not induce dark-line defects in the holographic image as captured in the retina image. (b) The wavefront alignment in the retina space should also be considered.
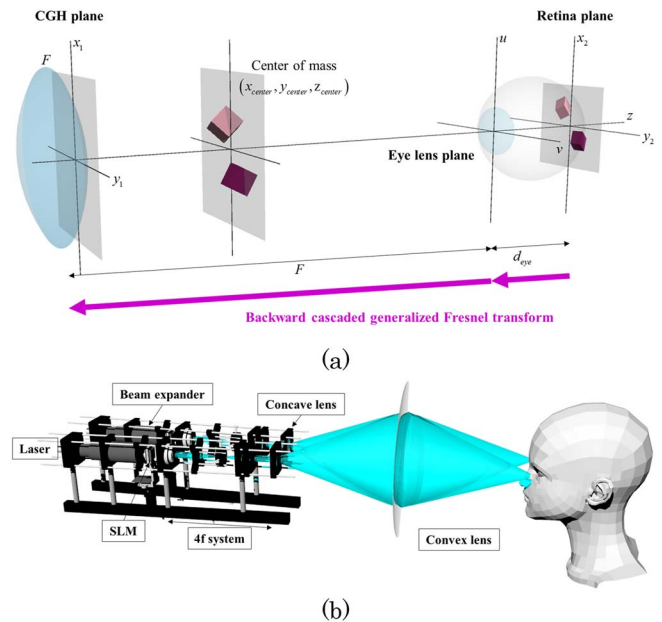

Fig. 3. (a) Optical system schematic of the eye observation of a holographic 3D image and (b) experimental setup of the holographic 3D display.

The triangular shapes with a thin axial dimension prevent abrupt differences in the normal vectors of the adjacent triangles. If the wavefront is set up to a flat piecewise continuous profile on the transformed object in the retina space, the wavefront profile of the object surface in the object space is automatically rendered satisfying the proposal described in Fig. 2(a).

In conventional polygon CGH synthesis [7,8], we should assign a phase value and a carrier wave direction to a triangular facet. Fortunately, in the proposed scheme, the assignment of a constant phase value to the triangular facets determines the wavefront alignment and carrier wave direction simultaneously.

The mathematical relationship between the CGH pattern, $G(x_1, y_1)$, in the CGH plane and the observed field, $F(x_2, y_2)$, in the retina plane is described by the cascaded generalized Fresnel transform. It takes the form of the cascaded double integral transform:

$$W(u, v; \lambda) = \mathrm{FrT}_1(G(x_1, y_1)). \tag{2a}$$

$$F(x_2, y_2; \lambda) = \mathrm{FrT}_2(t(u, v; \lambda)W(u, v)). \tag{2b}$$

The observer sees the holographic 3D scene from the CGH through the cascaded generalized Fresnel transform. The first stage transform of Eq. (2a) is defined by the modified Fresnel diffraction integral function as:

$$W(u, v; \lambda) = \frac{e^{jkF}}{j\lambda F} \iint G(x_1, y_1) e^{-j\frac{2\pi}{\lambda F}(x_1 u + y_1 v)} \mathrm{d}x_1 \mathrm{d}y_1. \tag{3a}$$

$W(u, v; \lambda)$ is the optical field distribution on the crystalline lens plane (u-v plane). FrT_1 is the modified Fresnel transform wherein the quadratic phase term, $e^{j\pi(u^2+v^2)/(\lambda F)}$ appearing in the conventional Fresnel transform, is detached for numerical stability. The second stage transform of Eq. (2b), FrT_2, is also defined by the modified Fresnel integral with an internal weight function $t(u, v; \lambda)$, which represents the optical wave propagation through an eye lens with focal length f_{eye}, defined by:

$$F(x_2, y_2; \lambda) = \frac{e^{j\frac{\pi}{\lambda d_{\mathrm{eye}}}(x_2^2 + y_2^2)}}{(j\lambda F)(j\lambda d_{\mathrm{eye}})}$$
$$\times \iint t(u, v)W(u, v) e^{-j\frac{2\pi}{\lambda d_{\mathrm{eye}}}(ux_2 + vy_2)} \mathrm{d}u \mathrm{d}v, \tag{3b}$$

where $t(u, v; \lambda)$ is the transmittance function given by:

$$t(u, v; \lambda) = A e^{j\frac{\pi}{\lambda}\left(\frac{1}{F} + \frac{1}{d_{\mathrm{eye}}} - \frac{1}{f_{\mathrm{eye}}}\right)(u^2+v^2)} \mathrm{circ}([u^2 + v^2]/\rho^2). \tag{3c}$$

Here $\mathrm{circ}([u^2 + v^2]/\rho^2)$ represents the finite eye aperture with a pupil radius of ρ [8]. The transmittance function merges the quadratic phase term, $e^{j\pi(u^2+v^2)/(\lambda F)}$, detached in Eq. (3a).

In the proposed algorithm, the observed field, $F(x_2, y_2; \lambda)$, for the projected 3D object, is first obtained in the retina plane (x_2-y_2 plane) by the polygon CGH algorithm and is transformed to the CGH plane through the inverse transform, as indicated in Fig. 3(a):

$$G(x_1, y_1) = \mathrm{IFrT}_1(t^{-1}(u, v; \lambda)\mathrm{IFrT}_2(F(x_2, y_2; \lambda))), \tag{4a}$$

where the internal transmittance function:

$$t^{-1}(u, v; \lambda) = e^{-j\frac{\pi}{\lambda}\left(\frac{1}{F} + \frac{1}{d_{\mathrm{eye}}} - \frac{1}{f_{\mathrm{eye}}}\right)(u^2+v^2)}. \tag{4b}$$

The inverse transforms, IFrT_1 and IFrT_2, can be straightforwardly derived from Eqs. (3a) and (3b). The quadratic phase function in the Fresnel transform allows a rendered curvature of the wavefront to be at the triangular facets by the buildup of a flat equiphase wavefront on the surface of the projected object in the retina space.

Figure 3(b) shows the experimental setup for optical reconstruction of CGH, which is composed of laser diodes with a wavelength of 633 nm, an SLM (EPSON LC-SLM L3C07U-85G10), and a field lens with a focal length of 460 mm. In the setup, the left and right beam lines are built up, with a laser source, a beam expander, and a 4-f Fourier filter for rejecting the conjugate and DC noise in the diffraction field. The optical projection part of a concave lens and a large diameter convex lens is used to create a conic volume space.

The CGH plane in Fig. 3(a) is the image of the SLM projected in the field lens plane. In this setup, the viewing window is fixed with a narrow viewing angle. The CGH pattern is imported into the SLM by the off-axis hologram format [14] and illuminated by the collimated laser light. The conjugate and the DC field are filtered out by the band-rejection filter in the 4-f system. In the experiment, the pictures of example holographic images are taken by a CMOS camera (Flea USB 3.0 made by Point Grey) along the single beam line, and image quality is inspected with respect to the accommodation effect and dark-line defect removal. The observer can watch the monocular parallax induced by the accommodation effect by changing the focal length of the eye lens, f_{eye}.
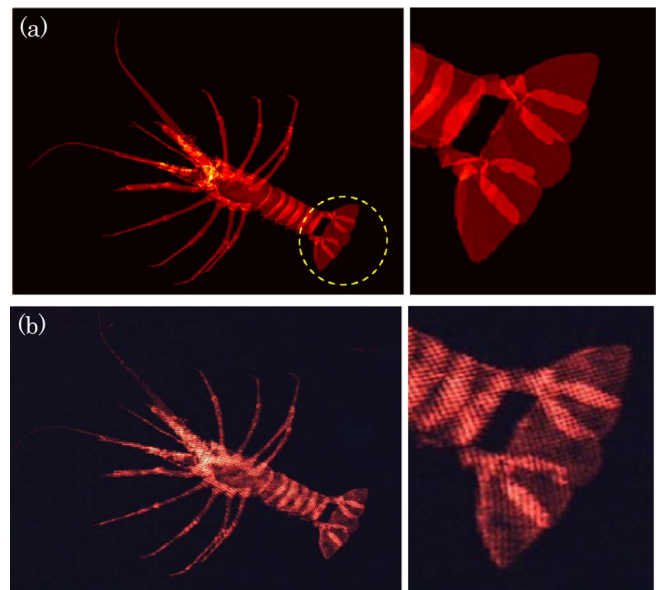

Fig. 4. 3D object generated by polygon CGH with phase-regularization (a) numerical simulation result and (b) experimental observation result.
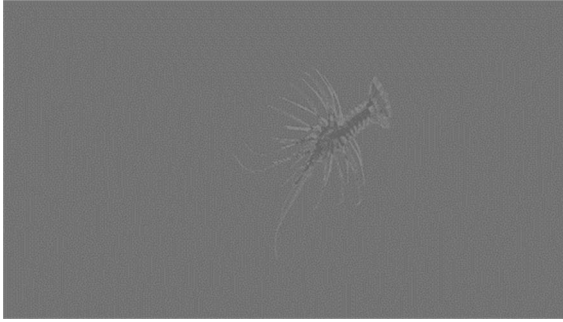
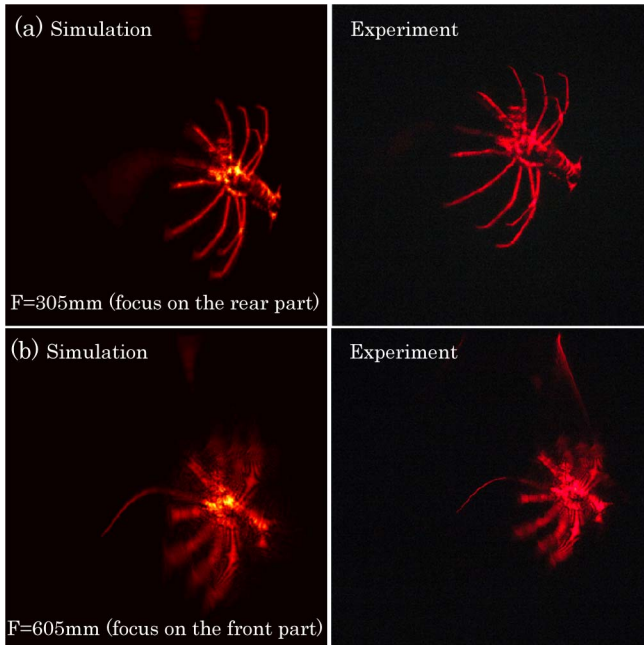Fig. 5.   Off-axis amplitude CGH pattern.

Fig. 6.   Comparison of the numerical and experimental observation results of a holographic 3D object when focused on its rear (a) and front (b).

In Fig. 4(a), the numerical result of the proposed phase-regularized polygon CGH algorithm is presented. A comparison with Fig. 1(a) clearly shows that the dark-line defects on the surfaces of the 3D object have been removed. Similar to the numerical simulation results, the dark-line defects are successfully removed in the experimental result in Fig. 4(b).

It is argued that the dark-line defects do not appear even with change in the eye focus and will be verified in the following experimental results. We perform an experimental observation of the depth discrimination of holographic 3D image, i.e., the accommodation effect. The off-axis amplitude CGH pattern for demonstration is shown in Fig. 5.

In Fig. 6, the experimental results demonstrating the depth discrimination of the holographic 3D images are presented with their corresponding numerical reconstruction results. In Fig. 6, the left and right images are the numerical and experimental reconstruction results, respectively. In Fig. 6(a), the observation focus is positioned at the rear of the object. In Fig. 6(b), when the focus is subsequently moved to the front, the feeler of the object is clearly observed in both the numerical and experimental results.

In conclusion, the proposed phase-regularized polygon CGH algorithm has been verified. In practice, many more polygons are necessary to detail the description of realistic 3D scenes. The proposed phase-regularization method would then enable the photorealistic holographic imaging of 3D objects.

References

1. H. Sasaki, K. Yamamoto, Y. Ichihashi, and T. Senoh, Sci. Rep. **4**, 4000 (2014).
2. B. Lee, Phys. Today **66**(4), 36 (2013).
3. J. Hong, Y. Kim, H. Choi, J. Hahn, J.-H. Park, H. Kim, S.-W. Min, N. Chen, and B. Lee, Appl. Opt. **50**, H87 (2011).
4. L. Onural, F. Yaras, and H. Kang, Proc. IEEE **99**, 576 (2011).
5. N. Takada, T. Shimobaba, H. Nakayama, A. Shiraki, N. Okada, M. Oikawa, N. Masuda, and T. Ito, Appl. Opt. **51**, 7303 (2012).
6. T. Shimobaba, T. Ito, N. Masuda, Y. Ichihashi, and N. Takada, Opt. Express **18**, 9955 (2010).
7. H. Kim, J. Hahn, and B. Lee, Appl. Opt. **47**, D117 (2008).
8. J. Cho, J. Hahn, and H. Kim, Opt. Express **20**, 28282 (2012).
9. K. Matsushima and S. Nakahara, Appl. Opt. **48**, H54 (2009).
10. K. Matsushima, H. Nishi, and S. Nakahara, J. Electron. Imaging **21**, 023002 (2012).
11. H. Nishi, K. Matsushima, and S. Nakahara, Appl. Opt. **50**, H245 (2011).
12. K. Matsushima, Appl. Opt. **44**, 4607 (2005).
13. T. Ichikawa, K. Yamaguchi, and Y. Sakamoto, Appl. Opt. **52**, A201 (2013).
14. E. Moon, M. Kim, J. Roh, H. Kim, and J. Hahn, Opt. Express **22**, 6526 (2014).